

Structural analysis of CuGeO_3 : Relation between nuclear structure and magnetic interaction

M. Braden

Forschungszentrum Karlsruhe, Institut für Nukleare Festkörperphysik, Postfach 3640, D-76021 Karlsruhe, Germany
and Laboratoire Léon Brillouin, CEA, CNRS, CE-Saclay, 91191 Gif sur Yvette Cedex, France

G. Wilkendorf

Institut für Kristallographie, Rheinisch-Westfälische Technische Hochschule Aachen, D-52056 Aachen, Germany

J. Lorenzana and M. Aïn

Laboratoire Léon Brillouin, CEA, CNRS, CE-Saclay, 91191 Gif sur Yvette Cedex, France

G. J. McIntyre

Institut Laue Langevin, Boîte Postale 156X, 38042 Grenoble Cedex, France

M. Behruzi and G. Heger

Institut für Kristallographie, Rheinisch-Westfälische Technische Hochschule Aachen, D-52056 Aachen, Germany

G. Dhalenne and A. Revcolevschi

Laboratoire de Chimie des Solides Orsay, Université Paris-Sud, 91405 Orsay Cedex, France

(Received 16 October 1995; revised manuscript received 29 January 1996)

The structure of CuGeO_3 has been analyzed by means of x-ray and neutron single-crystal diffraction as a function of temperature. There is a pronounced temperature dependency of the atomic positions in the high-temperature $Pbmm$ phase. The observed deformation scheme on cooling from 295 to 20 K may be characterized by a rotation of the $\text{Cu}[\text{O}(2)]_2$ ribbons around the c axis. It is related to the distortion below the spin-Peierls transition, and has an impact on the magnetic interaction parameter J . For the distorted structure in the spin-Peierls phase, based on a large set of superstructure reflections, we qualitatively confirm the proposed model (space group $Bbcm$) with a slightly different direction of the oxygen displacements. A computation of J reveals that its splitting in the spin-Peierls phase is dominated by the modulation of the Cu-O-Cu bond angle. [S0163-1829(96)00425-0]

I. INTRODUCTION

One-dimensional spin-1/2 systems have been the subject of an enormous amount of experimental and theoretical studies.¹ However, until recently, spin-Peierls (SP) transitions were known only in rather complicated organometallic structures. Therefore, the announcement by Hase, Terasaki, and Uchinokura² of an SP transition at 14 K in the inorganic, and rather simple compound CuGeO_3 stimulated a lot of additional work. The SP transition was further characterized by the magnetic phase diagram published by Hase *et al.*³ and by the magnetic-excitation spectrum determined by Nishi, Fujita, and Akimitsu.⁴ These observations seem to reproduce the expectations from the known organic compounds presenting a SP transition. However, the temperature dependence of the magnetic susceptibility deviates from the theory for a one-dimensional spin-1/2 system,⁵ which satisfactorily describes the organic systems.

Whereas the magnetic transition was rapidly confirmed, the structural component of the spin-Peierls transition remained subject to controversial discussion. By neutron diffraction Nishi⁶ observed additional intensities at rather low temperatures. However, with the same method Lorenzo *et al.*⁷ could not confirm these reflections in a crystal which

clearly exhibits the SP transition. Pouget *et al.*⁸ showed that the reflections found by Nishi *et al.* are not characteristic for the spin-Peierls transition but for antiferromagnetic order, which occurs in some crystals not presenting the SP transition. Later, a detailed study of the $\text{CuGe}_{1-x}\text{Si}_x\text{O}_3$ system revealed a competition between the SP transition and this type of antiferromagnetic order.⁹

An indication for the structural distortion in the SP phase was found by combined x-ray- and neutron-diffraction studies by Pouget *et al.*,⁸ who observed superstructure reflections of the type $(h/2kl/2)$. The same type of superstructure reflection was also seen in electron-diffraction experiments.¹⁰ A detailed analysis of the observed reflections led Kamimura *et al.* to the conclusion that the distorted nuclear structure of the SP phase in CuGeO_3 should belong to space group $Bbmm$ or $Bbcm$.¹⁰ A collection of 11 superstructure reflections in the SP phase by neutron diffraction allowed Hirota *et al.*¹¹ to determine the space group to be $Bbcm$ in accordance with the electron-diffraction results.

The high-temperature structure was determined properly by Völlenklee, Wittman, and Nowotny;¹² the space group is $Pbmm$ (standard setting $Pmma$). The structure consists of CuO_6 octahedra and GeO_4 tetrahedra stacked along the c direction, see Fig. 1. Each oxygen belongs to a Ge tetrahe-

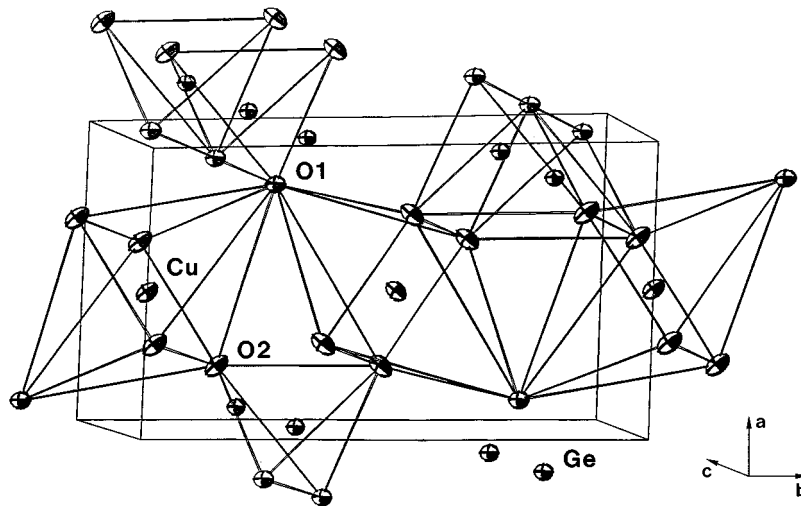


FIG. 1. ORTEP plot of the room-temperature structure of CuGeO_3 as determined by neutron diffraction. The ellipsoids represent 40% probability density. The lines indicate the lattice according to $Pbmm$; for clarity a set of atoms is shown which corresponds to more than one unit cell.

dron and to a Cu octahedron. The stacking of the edge-sharing octahedra results in chains with rather short Cu-Cu distances. The tetrahedra are also chained along one of their edges. As CuGeO_3 is now commonly compared to the high- T_c cuprates, it seems interesting to note that there is an important difference between the crystal structures. Whereas the cuprate structures are completely filled by the different types of cation anion polyhedra, there exist rather large empty cavities in the case of CuGeO_3 .

The importance of the nuclear structure on the magnetism in CuGeO_3 was revealed in different experiments. Lorenzo *et al.*⁷ showed that the SP transition is accompanied by a spontaneous strain along b . By high-resolution thermal-expansion measurements Winkelmann *et al.*¹³ confirmed the existence of giant spontaneous strains along all three orthorhombic directions. The strong implication of the nuclear structure was further confirmed by large anomalies in the ultrasound velocities.¹⁴ Furthermore, there are indications that the crystal structure is rather anharmonic even above the SP transition. The longitudinal-acoustic branch along b was found to be rather soft,⁷ which seems to reflect the large compressibility of CuGeO_3 in this direction.¹⁵ At high pressure CuGeO_3 even presents a purely structural phase transition.¹⁵ The thermal expansion above T_{SP} is anisotropic and exhibits extrema along a and c ; Winkelmann *et al.* speculate that this behavior might be related to the unexplained temperature dependence of the magnetic susceptibility.¹³ A more detailed knowledge of the temperature dependence of the nuclear structure seemed, therefore, desirable.

In this paper we present the results of single-crystal diffraction studies as function of temperature. We will show that there are significant temperature dependences in the crystal structure already above T_{SP} . CuGeO_3 appears unstable against twist or rotation deformations of the $\text{Cu}[\text{O}(2)]_2$ ribbons just above and at T_{SP} . The influence of the nuclear arrangement on the magnetic interaction parameters will be analyzed in detail.

II. EXPERIMENTAL

Stoichiometric CuGeO_3 was prepared from the oxides CuO and GeO_2 (with 99.99% purity) and pressed into cylin-

dric rods. After sintering at 1000 °C for 24 h these rods were used in order to grow large single crystals of CuGeO_3 by a traveling floating-zone technique using an image furnace.¹⁶ Identically prepared crystals were used in a large number of different experiments (for example, see Refs. 8, 9, 13, 14, and 17); the spin-Peierls transition was found to occur at 14.4 K.⁸ The phase diagram of CuO/GeO_2 gives no indication for any solid solution deviating from the CuO/GeO_2 1/1 ratio;¹⁸ so unstoichiometry may be introduced mainly by improper starting oxides, which, however, can be excluded in our procedure. The ideal stoichiometry of our crystals was verified by electron microprobe analysis and by inductively coupled plasma atomic emission spectroscopy; both techniques confirm an ideal stoichiometry within their precision.

The crystals grow as cylindrical rods parallel to a with the basal plane being elongated along c ; they cleave easily along the b, c plane. For the neutron-diffraction studies small crystals were cut out of the as-grown ones. About 15 different smaller samples were tested on several diffractometers at LLB and ILL; however, it turned out that all of them were far from perfect. Two different types of imperfection were observed, one being a misalignment of different parts of the crystal characterized by a rotation around a , i.e., the axis of crystal growth. This imperfection seems to be related to the cleavability. The second type consists in an enhanced mosaicity or misalignment of crystallites in the a, c plane (rotation around b); thin crystals can even be bent around the b axis without cracking. These imperfections are both likely to be related to the CuGeO_3 crystal structure. For the neutron-diffraction study we chose finally a rectangular crystal of $5.5 \times 4.5 \times 0.8 \text{ mm}^3$ with a mosaicity (background to background) of slightly less than 2° . The crystal used for the x-ray-diffraction study was much smaller, about $0.09 \times 0.05 \times 0.05 \text{ mm}^3$, and no peak broadening was observed.

The x-ray experiment was performed on a CAD4 four-circle diffractometer using $\text{Mo } K\alpha$ radiation ($\lambda = 0.711 \text{ \AA}$); a half sphere of 7141 reflections was measured up to $\Theta = 60^\circ$. A numerical absorption correction was applied according to the shape of the sample crystal ($\mu = 226 \text{ cm}^{-1}$).

The neutron-diffraction study was performed on the four-circle diffractometer D10 at ILL using a wavelength of 1.26

\AA obtained by a Cu (200) monochromator. The crystal was glued with its c axis roughly parallel to the ϕ axis of the diffractometer. The orientation matrix was determined by centering a set of 20 reflections. The enlarged mosaicity of the crystal had to be taken into consideration in order to assure complete integration of the Bragg intensities. The scan width was adapted according to the Θ /scanwidth table: $0^\circ/3.5^\circ$; $15^\circ/3.5^\circ$; $30^\circ/3.5^\circ$; $45^\circ/3.5^\circ$; $80^\circ/5.5^\circ$. Due to the small take-off angle of the monochromator the ω resolution decreases rapidly for increasing scattering angle; so, the integration of the Bragg reflection intensities remains complete for switching to the coupled ω - $x\Theta$ scan mode. The coupling parameter of the ω - $x\Theta$ scan was chosen as usually according to the Θ/x table: $0^\circ/0$; $15^\circ/0.75$; $30^\circ/1.3$; $45^\circ/1.9$ and $65^\circ/2.0$.

The sample was mounted in a liquid-helium cryostat and cooled down to 4 K, where the orientation matrix was determined with the same reflections as at room temperature. The fundamental reflections were measured in the same configuration as at room temperature but with reduced counting time. Superstructure reflections were measured according to the $2a \times b \times 2c$ lattice; however, only a few reflections forbidden by the B centering were measured, none of them was observable. A complete set of superstructure reflections was measured only up to $2\Theta = 70^\circ$ with strongly enhanced counting time (~ 30 s); first calculations during the measurement indicated an agreement with the proposed model, i.e., space group $Bbcm$. Therefore, it seemed reasonable to concentrate these highly time-consuming measurements on the superstructure reflections which the model predicted to be strongest. The intensity of the superstructure reflections being in the order of magnitude of the background the exact determination of the latter is essential. However, as the background is strongly varying with 2Θ due to the powder lines from the cryostat and sample support materials, it can be properly obtained only by pure ω scans. Therefore, we had to use this scan technique for the superstructure reflections. Tests on fundamental reflections showed that the ω scan cuts significantly intensity only for 2Θ larger than 100° ; at $2\Theta = 120^\circ$ one loses about 4% of intensity which is not essential for the superstructure reflections. Only very few superstructure reflections were measured at high 2Θ values; their intensities should mainly influence the thermal parameters which are adjusted with much higher statistics by the fundamental reflections. Therefore, the error coming from this scan mode can certainly be neglected. Figure 2 shows superstructure reflection scans compared to their analogs at 20 K.

A small data set of fundamental reflections was collected at 20 K using the 4 K orientation matrix; scan parameters were identical as for the other temperatures, only the counting time was further reduced. Additionally, some of the strongest superstructure reflections were remeasured with enhanced counting time. All neutron data sets were corrected for absorption numerically.

III. STRUCTURAL REFINEMENTS

All structural refinements were performed with the PROMETHEUS program package.¹⁹ An extinction correction was applied according to the Becker Coppens formalism corresponding to secondary extinction of type I with an isotro-

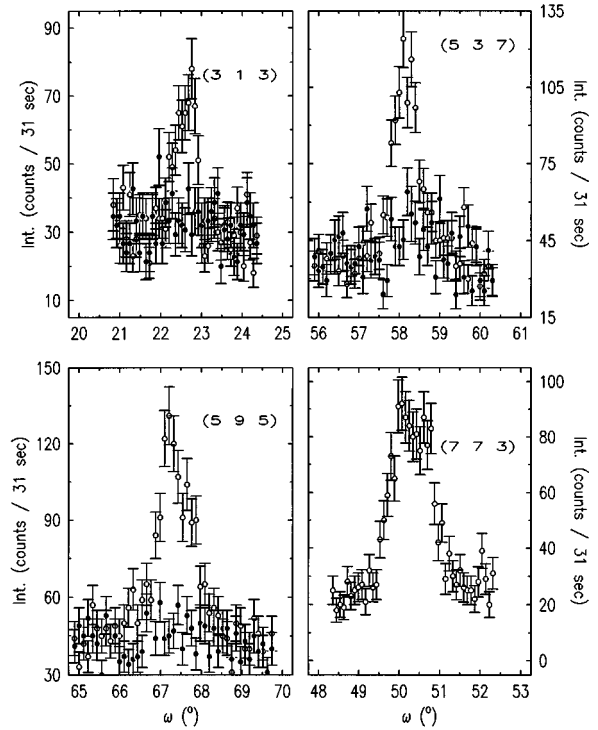


FIG. 2. Intensity distribution of the ω scans through some superstructure reflections of the spin-Peierls phase; above (20 K, closed circles), and below T_{SP} (4 K, open circles).

pic Lorentzian distribution of the mosaicity.

X-ray diffraction at 295 K—The reflections of the x-ray data set were averaged to 1036 independent reflections of which 745 were stronger than 2σ ; the internal R value was 4.25%. The refinement was performed using the statistical weights; the structural model according to space group $Pbmm$ converged rapidly without strong correlations. The positional parameters displayed in Table I are in agreement with the earlier work by Völlenkle, Wittmann, and Nowotny¹² and with more recent neutron powder-diffraction studies.^{20,21}

Neutron diffraction at 295 K—The 580 reflections measured at room temperature on the neutron diffractometer D10 were averaged to 291 independent ones according to mmm ; the obtained internal R value of 3.30% confirms the complete integration of the Bragg intensities. Due to the large sample volume the observed integrated intensities are rather high, up to 150.000 counts per 3 s. As consequence the statistical errors predict an internal R value lower than the one which was obtained. Therefore, we had to choose a modified weighting scheme for the refinements. There are different sources of additional errors which alter the reliability of the measured Bragg reflection intensities in the case of large crystals. Extinction and integration problems should roughly be proportional to the intensity, I . Therefore, they can be taken into account by adding a term proportional to the reflection intensity, $\text{ign} \times I$, to the square of the statistical error σ_{stat}^2 . Additionally, there is an almost uniform probability for contamination by multiple diffraction. Some of the reflections forbidden in $Pbmm$ were in fact clearly observed; it was, however, verified that they are induced by multiple diffraction by rotating the crystal around the scattering vector.

TABLE I. Results of the different single-crystal structural analyses. The estimated standard deviations in the last digits are given in parentheses. The lattice constants at 20 K have been determined by combining the 4 K values with the highly precise $\Delta L/L$ results from Ref. 13.

	X ray 295 K	Neutron <i>D</i> 10 295 K	Neutron <i>D</i> 10 20 K	Neutron <i>D</i> 10 4 K
<i>a</i> (Å)	4.801(1)	4.795 6(13)	4.789 28	2×4.789 4(12)
<i>b</i> (Å)	8.469(2)	8.466(4)	8.402 56	8.401 8(44)
<i>c</i> (Å)	2.943 1(4)	2.940 4(13)	2.944 47	2×2.944 5(13)
Ind. Refl.	1034	291	103	374
$R_w(F^2)$ (%)	3.28	3.39	3.33	4.22
$R_{uw}(F^2)$ (%)	3.26	3.00	2.88	3.60
Cu <i>x</i>	0.5	0.5	0.5	0.0
<i>y</i>	0.0	0.0	0.0	0.0
<i>z</i>	0.0	0.0	0.0	0.250 96(3)
<i>U</i> 11	0.010 6(1)	0.012 3(3)	0.004 7(5)	0.003 3(3)
<i>U</i> 22	0.013 3(1)	0.015 1(3)	0.005 4(9)	0.004 0(3)
<i>U</i> 33	0.003 9(1)	0.005 4(3)	0.001 5(7)	0.002 6(3)
<i>U</i> 12	0.005 1(1)	0.004 9(2)	0.000 4(4)	0.001 1(3)
Ge <i>x</i>	0.074 33(4)	0.074 38(13)	0.071 3(2)	−0.214 58(8)
<i>y</i>	0.25	0.25	0.25	0.249 91(3)
<i>z</i>	0.5	0.5	0.5	0.0
<i>U</i> 11	0.006 0(1)	0.008 0(3)	0.003 7(5)	0.002 7(3)
<i>U</i> 22	0.009 7(1)	0.010 6(3)	0.003 5(10)	0.003 1(3)
<i>U</i> 33	0.002 9(1)	0.005 0(3)	0.003 5(8)	0.002 5(3)
O(1) <i>x</i>	0.868 1(3)	0.867 7(2)	0.863 9(3)	0.182 06(11)
<i>y</i>	0.25	0.25	0.25	0.25
<i>z</i>	0.0	0.0	0.0	0.25
<i>U</i> 11	0.007 4(4)	0.008 7(4)	0.005 6(6)	0.003 8(4)
<i>U</i> 22	0.012 2(5)	0.013 6(4)	0.005 0(13)	0.005 6(4)
<i>U</i> 33	0.003 6(4)	0.006 1(3)	0.003 1(10)	0.003 5(4)
O(2 <i>a</i>) <i>x</i>	0.283 2(1)	0.283 50(15)	0.281 6(2)	−0.108 26(8)
<i>y</i>	0.083 2(1)	0.083 16(8)	0.081 9(2)	0.082 90(10)
<i>z</i>	0.5	0.5	0.5	0.0
<i>U</i> 11	0.013 5(4)	0.015 3(3)	0.006 0(4)	0.005 3(3)
<i>U</i> 22	0.017 0(4)	0.018 7(3)	0.010 0(10)	0.005 7(3)
<i>U</i> 33	0.005 1(3)	0.007 1(3)	0.002 9(8)	0.003 8(3)
<i>U</i> 12	0.008 0(3)	0.007 7(2)	0.001 3(3)	0.001 9(2)
O(2 <i>b</i>) <i>x</i>				−0.110 25(8)
<i>y</i>				0.081 36(10)
<i>z</i>				0.5
<i>U</i> 11				= <i>U</i> 11-O(2 <i>a</i>)
<i>U</i> 22				= <i>U</i> 22-O(2 <i>a</i>)
<i>U</i> 33				= <i>U</i> 33-O(2 <i>a</i>)
<i>U</i> 12				= <i>U</i> 12-O(2 <i>a</i>)

Similar multiple-diffraction effects could explain also the observation of forbidden reflections by Arrai *et al.* on an even larger crystal.²² This error source can be accounted for by adding a constant term, const, resulting in $\sigma_{\text{new}}^2 = \sigma_{\text{stat}}^2 + \text{ign} \times I + \text{const}$. For the room-temperature data set $\text{ign} = 0.01$ and $\text{const} = 400$ seemed to be the appropriate choice. Using these weights the room-temperature structure was easily refined with satisfying agreement; the results are given in Table I. There is excellent agreement between the neutron and x-ray results concerning the positional parameters (within the errors). Also the anisotropic mean-square displacements confirm each other. That the neutron values are slightly larger might be due to approximations in the absorp-

tion corrections or to different contributions from thermal diffuse scattering.

Neutron diffraction at 4 and 20 K—Since the room-temperature experiment showed that the quality of the data is not limited by counting statistics, the counting time for the 4 and 20 K data collections was reduced. Hence, the factor ign could be reduced to 0.005 and 0.003, respectively. Extinction and multiple-diffraction effects cannot affect the weak superstructure reflections appearing below the SP transition. Therefore, their σ 's remained unchanged. These reflections get higher weight in the refinements due to their typically 10–20 times higher counting rate. The 635 measured reflections were averaged to a set of 374 independent ones of

TABLE II. Atomic site symmetries of the atoms in CuGeO_3 in the high-temperature phase (space group $Pbmm$) and in the spin-Peierls phase (space group $Bbcm$). The $Bbcm$ lattice is obtained from the $Pbmm$ one by doubling a and c and shifting the origin by $(0.25\ 0\ 0.25)$.

	$Pbmm$		$Bbcm$	
Cu	$(\frac{1}{2}/0/0)$	$2b$	$(0/0/\frac{1}{4} + \Delta z)$	$8d$
Ge	$(x/\frac{1}{4}/\frac{1}{2})$	$2f$	$(\frac{x}{2} - \frac{1}{4}/\frac{1}{4} + \Delta y/0)$	$8f$
O(1)	$(x/\frac{1}{4}/0)$	$2e$	$(\frac{x}{2} - \frac{1}{4}/\frac{1}{4})$	$8e$
O(2)	$(x/y/\frac{1}{2})$	$4j$	$(\frac{x}{2} - \frac{1}{4} + \Delta x/y + \Delta y/0)$	$8f$
O(2b)			$(\frac{x}{2} - \frac{1}{4} - \Delta x/y - \Delta y/\frac{1}{2})$	$8f$

which 84 are superstructure reflections; the internal R value for this data set, 3.68%, is comparable to the one obtained at room temperature indicating a similar quality of both sets and hence a reliable determination of the superstructure intensities. Due to the enormous difference in the intensity of superstructure and fundamental reflections (a factor of 10^3 – 10^4) it was necessary to correct the data for $\lambda/2$ contamination. The amount of $\lambda/2$ radiation was determined by analyzing pairs of (hkl) and $(h/2k/2l/2)$ with k odd in the $Pbmm$ lattice; the observed ratio amounts to 0.000 20(3) on F^2 . The correction was performed during the refinement by calculating a superposition $0.9998F^2(hkl) + 0.0002F^2(2h\ 2k\ 2l)$ similar to the technique used in the case of twinned crystals.²³ Satisfying agreement to the data could be obtained with the space group $Bbcm$ proposed by Hirota *et al.*¹¹ The structure according to $Bbcm$ (standard setting $Cmca$) has the same orientation of the crystal axes as in the high-temperature phase $Pbmm$; for instance the c direction remains the direction of the chains. However, the lattice is doubled along a and c with respect to $Pbmm$ and the origin is shifted by 0.25 along a and c . Table II reviews the different site symmetries in $Bbcm$. In contrast to the work by Hirota *et al.* our data allows independent refinement of all positional parameters. There is a rather small shift of the Ge site, and O(2a) and O(2b) can be refined without any restriction. The other space group proposed by Kamimura *et al.*,¹⁰ $Bbmm$ was also tested. Whereas a similar description of the fundamental reflections can be achieved in $Bbmm$, the entire set including the superstructure reflections yields the much larger agreement factor, $R_w(F^2) = 9.8\%$; the $Bbmm$ space group can be definitely excluded.

The small data set measured at 20 K contained only a few symmetrically equivalent reflections; the 20 K structure was refined as the room-temperature phase against the 103 averaged reflections.

IV. DISCUSSION

A. High-temperature phase

Figure 1 shows an ORTEP plot of the room-temperature structure of CuGeO_3 as determined by our neutron-diffraction experiment. There is a good agreement with the other diffraction data; however, we obtain better precision especially for the anisotropic mean-square displacements. The two elements of the CuGeO_3 structure are displayed

separately in Fig. 3. The GeO_4 tetrahedron is almost perfect with roughly equal Ge-O distances and O-O edges. Furthermore, the different bond angles of type O-Ge-O are all close to the ideal tetrahedral value. The minor deviations reflect the fact that each O(1) belongs to two tetrahedra and each O(2) only to one. The calculation of the bond-valence sum according to the formalism of Brown and Altermatt²⁴ yields a value of 3.956 which is very close to the expected value of 4.00 for tetravalent Ge. All this information together indi-

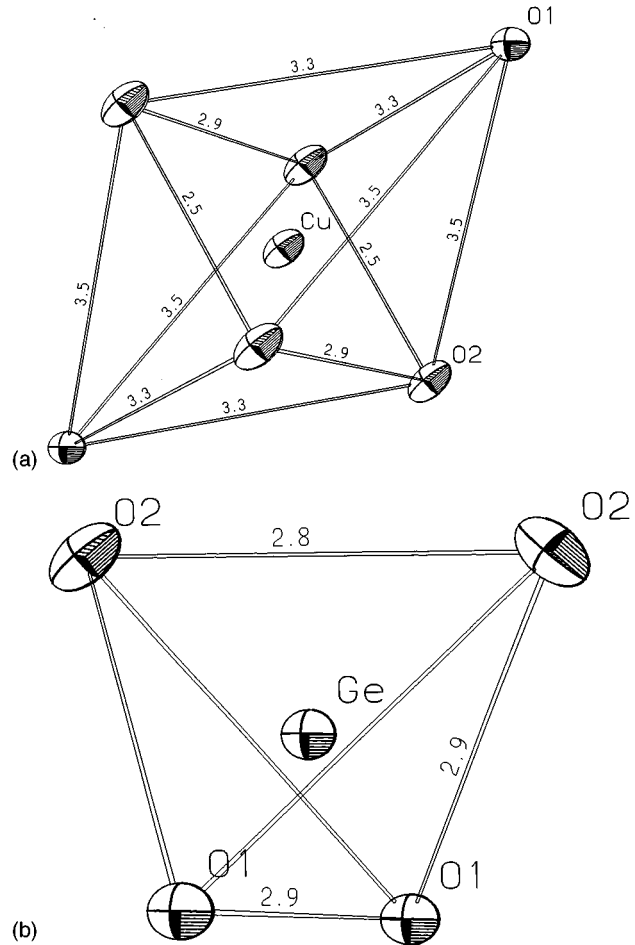


FIG. 3. Representation of the two elements constituting the CuGeO_3 structure, the CuO_6 octahedron and the GeO_4 tetrahedron; here the thermal ellipsoids present 50% probability density. The orientation of the crystal lattice and the viewing direction is identical to the one in Fig. 1.

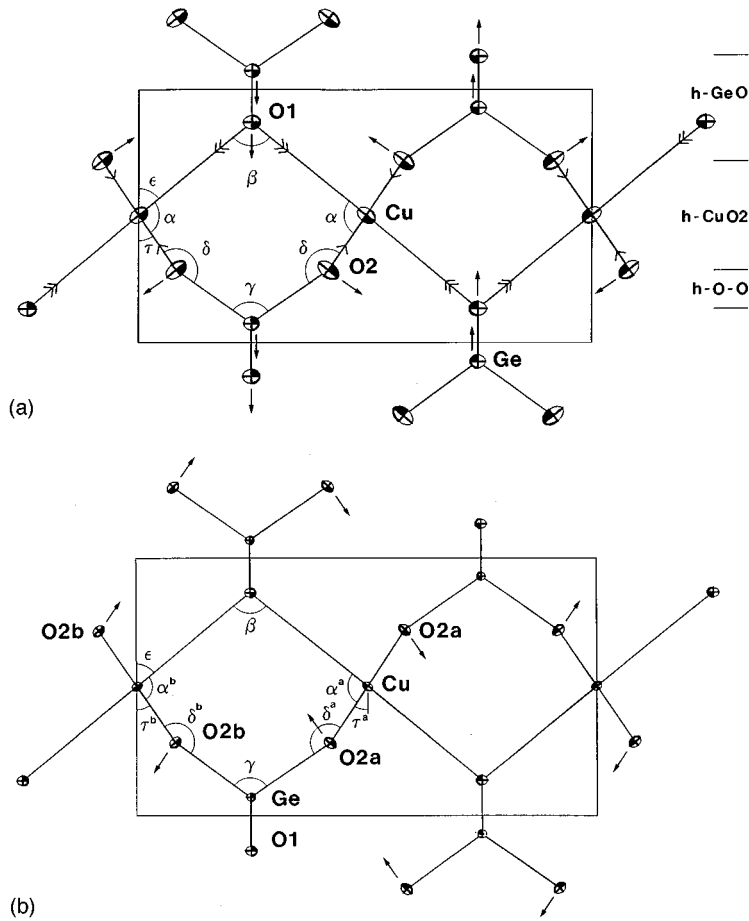


FIG. 4. (a) Projection of the CuGeO₃ structure at room temperature on the *a,b* plane in form of an ORTEP plot (the *a* direction is vertical); the arrows indicate qualitatively the shift of the atomic positions on cooling to 20 K. Note, that the deformation on cooling is accompanied by a strong reduction of the *b* lattice parameter. (b) identical as (a) for the low-temperature structure at 4 K in the spin-Peierls phase. The symbols represent the exact atomic positions, the arrows illustrate the displacements with respect to the high-temperature *Pbmm* phase. The figure presents only atoms with $0.25 < z \leq 0.5$. In both figures the lines indicate the high-temperature *Pbmm* lattice.

icates an undistorted GeO₄ structure; if there is any internal strain present in CuGeO₃ it is unable to deform substantially the rather rigid tetrahedron. On the contrary the CuO₆ octahedron is rather distorted. The CuO(1) bond is not perpendicular to the Cu[O(2)]₄ basal plane, $\alpha = 95.66^\circ$, giving rise to two different edge lengths O(1)-O(2), see Fig. 3. Furthermore, the basal plane itself is strongly deformed; the ratio of the long to the short O(2)-O(2) edge is 1.2. Consequently the Cu-O(2)-Cu angle η is far away from 90° . As is discussed below, it is this deviation which seems to be essential for the strength of the magnetic interaction. The bond-valence sum for Cu gives only a slightly increased value of 2.12, compared to the expected value of 2.00.²⁴ So, the strong deformation of the CuO₆ octahedron is realized mainly in shear stresses, whereas there seems to exist almost no volume effect.

The mean-square displacements of the GeO coordination possess rather small components parallel to the Ge-O bonds in accordance with their strong and covalent nature. Also most of the other thermal parameters appear reasonable in magnitude compared to similar structures. The O(1) site shows almost isotropic thermal parameters due to its homogeneous surroundings. However, Cu and O(2) are definitively anisotropic. The displacement of Cu perpendicular to the octahedron basal plane formed by the O(2)'s is significantly enhanced which may be explained by the large Cu-O(1) distance. The Cu-O(1) bond appears too weak in order to fix the Cu ion effectively. The largest amplitude of the thermal ellipsoid of the O(2) ion is even higher. This can be best seen in the projection of the structure on the *a,b* plane

in Fig. 4(a). The largest amplitude amounts to 0.158 Å and is almost perpendicular to the projections of the Cu-O(2) bonds from the two Cu sites at $z = \pm 0.25$. In contrast, the elongation of the O(2) thermal ellipsoid is not at all perpendicular to the projection of the Ge-O(2) bond. The large value and the direction of the elongation might indicate the proximity to a structural instability which might be characterized by a rotation or twisting of the O(2)-O(2) edges around the *c* axis.

The 20 K refinement evidences significant changes in the structure of the *Pbmm* phase on cooling. The *Pbmm* phase has several free positional parameters whose variation can modify the structural arrangement drastically without changing the symmetry.

First indications for a rather anomalous temperature dependency were found in thermal-expansion measurements which showed a pronounced anisotropy.¹³ There is a significant volume reduction between 295 and 20 K, $\Delta V/V = 0.0074$, whereas almost all cation-anion distances increase on cooling, see Table III. Only the Cu-O(1) distance decreases; however, the shortening by about 1% appears too strong compared with other cuprate structures. This means that the volume thermal expansion is realized not homogeneously but mainly in the empty cavities between the octahedra and the tetrahedra.

Figure 4(a) shows qualitatively the positional shifts occurring on cooling from 295 to 20 K in the projection on the *a,b* plane. The main effect can be characterized by a rotation of the Cu[O(2)]₄ squares around the *c* axis (the τ angle decreases by about 0.8°), and is in fact the motion where indications for instability were already found in the thermal pa-

TABLE III. Bond lengths and angles for the three temperatures, the notation of some angles is illustrated in Fig. 4.

	295 K	20 K	4 K
a (Å)	4.7956(13)	4.7893(13)	4.7894(12)×2
b (Å)	8.466(4)	8.403(4)	8.402(4)
c (Å)	2.9404(13)	2.9445(13)	2.9445(13)×2
Cu-O(1)	2.7549(8)	2.7295(12)	2.7300(10)
Cu-O(2)	1.9326(7)	1.9327(10)	(a)1.9351(7)/(b)1.9322(8)
Val. Cu	2.125	2.132	2.127
Ge-O(1)	1.7730(8)	1.7761(11)	1.7742(9)
Ge-O(2)	1.7322(10)	1.7345(17)	(a)1.7346(10)/(b)1.7338(11)
Val-Ge	3.956	3.928	3.939
O(1)-O(1)	2.9404(13)	2.9445(13)	2.9445(13)
O(1)-O(2)	2.8516(11)	2.8573(15)	(a)2.8588(12)/(b)2.8519(11)
O(2)-O(2) (in tetrah.)	2.8249(18)	2.824(4)	2.8209(18)
O(2)-O(2) (c)	2.9404(13)	2.9445(13)	2.9446(13)
O(2)-O(2) (a, b)	2.5089(16)	2.504(2)	(a)2.4984(17)/(b)2.5159(17)
α -[O(1)-Cu-O(2)] _{proj.}	95.66(3)	96.33(3)	α^a 95.81(5)/ α^b 96.77(5)
β -[Cu-O(1)-Cu]	100.39(4)	100.64(5)	100.60(4)
γ -[O(2)-Ge-O(2)]	109.25(6)	109.01(10)	108.84(6)
δ -[Cu-O(2)-Ge] _{proj.}	159.52(6)	158.85(11)	δ^a 159.86(6)/ δ^b 158.10(6)
ϵ -[Cu-O(1)/ a]	50.20(2)	50.32(2)	50.30(2)
φ -[O(1)-Ge-O(1)]	112.04(5)	111.97(10)	112.16(7)
φ' -[O(1)-Ge-O(2)]	108.88(2)	108.95(3)	φ'^a 109.16(2)/ φ'^b 108.73(2)
τ -[O(2)-O(2)/ a]	34.14(2)	33.36(3)	τ^a 33.89(4)/ τ^b 32.91(4)
η -[Cu-O(2)-Cu]	99.06(4)	99.24(5)	η^a 99.59(4)/ η^b 98.76(4)

rameters. The rotation is accompanied by a shift of the entire GeO_4 tetrahedron along a . The strong thermal expansion along b can be understood due to the rigid rotation of the $\text{Cu}[\text{O}(2)]_4$ squares, the width of the tetrahedra [corresponding to the O(2)-O(2) distance] being almost rigid (see Table III). However, the reduction of the b lattice parameter is possible only with the concomitant decrease of the CuO(1) bond, which is indeed enormous, -1% . The possibility of reducing the lattice volume by reducing b seems to be the driving force for the temperature-dependent rearrangement.

Along a a substantial but much lower positive thermal expansion is observed, see Table I and Ref. 13. The a parameter can be decomposed into three components, see Fig. 4(a): the height of the tetrahedron which increases on cooling, the projection of the $\text{Cu}[\text{O}(2)]_4$ square which increases too, and the small projection of the O(2)-O(1) distance which strongly decreases, due to the fact that the tetrahedra are shifted closer together. Inspection of the $\text{Cu}[\text{O}(2)]_4$ projection in detail shows that the increase of the octahedron edge projection is much smaller than what should be expected for a rigid rotation. This octahedron edge (parallel to the a, b plane) is additionally shortened which can be easily explained due to the enhanced pressure introduced by the closer GeO_4 tetrahedra. The compression of the O(2)-O(2) distance parallel to the a, b plane is, however, compensated by the elongation of the O(2)-O(2) edge along c ; the average of both edges remains constant. As discussed below, the change of this edge length ratio should further influence the magnetic interaction parameter J .

To summarize the structural deformation on cooling, one may argue that there is a rotation or twisting of the O(2)-

O(2) octahedron edges accompanied by a translation of the tetrahedron which cause smaller additional deformations. The reason for this behavior might be an internal mismatch between the sizes of the octahedra and the tetrahedra on one side and the volumes of the empty cavities on the other. However, it cannot be ruled out that the magnetic interaction itself is responsible for the anharmonic structural behavior. The instability seems further to be related to the observed compressibilities,¹⁵ which are largest along b , less along a and smallest along c , and which, hence, reflect perfectly the temperature dependences.

B. Spin-Peierls phase

The structure analysis of the spin-Peierls phase confirms the structural model proposed by Hirota *et al.*¹¹ qualitatively. However, Hirota *et al.* estimated the basic structure from the literature data available for 295 K, and their refinements were based on only seven superstructure reflection intensities with $I/\sigma > 3$. The differences between our results and Ref. 11 are easily explained due to the more complete set of superstructure reflection intensities and a more appropriate description of the fundamental structure. Whereas we agree with the shift of the Cu site along c , $\Delta z = 0.000\,96(3)$, and the one of the O(2) site along a , $\Delta x = 0.000\,99(6)$, even quantitatively, there is a significant difference in the O(2) shift along b , Δy . We observe $\Delta y = 0.000\,77(6)$ in contrast to the value $0.001\,25(6)$ which was obtained in Ref. 11. Note, that our refinement is free from any constraints; if we introduce the constraint used by Hirota *et al.*, the error bars of Δx and Δy are reduced by a factor of 4 without any shift

of the values. Our Δy value indicates that the O(2) sites are shifted almost perpendicular to the Ge-O(2) bonds, see Fig. 4(b), and not perpendicular to the O(2)-O(2) octahedron edges.

The displacement pattern of the SP phase with respect to the high-temperature structure is illustrated in Fig. 4(b). In contrast to the distortion between 295 and 20 K there is a doubling of the lattice parallel to a and c . Hence, the distortion cannot be described by a simple $\text{Cu}[\text{O}(2)]_4$ square rotation; the O(2) edges below and above a Cu site are twisted in opposite senses. As a simple description one may characterize the distortion as a rotation of the GeO_4 tetrahedron around their c axis with neighboring tetrahedra being rotated in opposite senses. The O(2) site of the Pbm phase splits into two distinct sites in the SP phase which can be seen in Fig. 4(b). The O(2a) site is displaced in the sense that the δ^a angle corresponding to the Cu-O(2a)-Ge projection comes closer to 180° ; concomitantly the O(2a)-O(2a) distance becomes shorter. The O(2b) site is shifted in the opposite sense thereby decreasing δ^b and increasing the O(2b)-O(2b) distance.

Note, however, that the average O(2)-O(2) distance parallel to the a, b plane is slightly increased, whereas the height of the octahedron basal plane decreases on passing into the spin-Peierls phase. Thus, these distances behave just in an opposite way in the normal phase and at T_{SP} . In this sense, they reflect the behavior of the lattice parameters a and c whose temperature dependences were similar in magnitude but opposite in sign both above and at T_{SP} .¹³ It seems reasonable to assume that the temperature dependences of the lattice parameters result from the behavior of the O(2)-O(2) octahedron edges. In the high-temperature phase the c parameter corresponds directly to the length of the O(2)-O(2) edge parallel c . It also seems reasonable to assume that the ratio of height-to-average-width of the $\text{Cu}[\text{O}(2)]_4$ square can respond to the internal strains on cooling and at T_{SP} quite easily, whereas the area of the $\text{Cu}[\text{O}(2)]_4$ square remains more or less fixed, thereby explaining the thermal-expansion observations. The edge ratio can be compared to the orthorhombic strain observed in La_2CuO_4 which reflects the splitting of the CuO_6 octahedron edge lengths in this structure. The orthorhombic strain and the edges vary essentially due to the structural phase transition in La_2CuO_4 , whereas the area of the planes is almost temperature independent.²⁵

The Cu ions themselves are shifted towards the O(2b) edges which are elongated; hence, their shift reduces the splitting of the Cu-O(2) distances which remains rather small. The distortion pattern in the SP phase is optimized in order to obtain a large difference in the Cu-O(2)-Cu bond angle, η , which produces a large splitting in J as discussed below.

First inspection of the displacement pattern in the spin-Peierls phase seems to indicate little similarity to the temperature-dependent deformation above T_{SP} . However, the rotation of the O(2) edges around the c axis is the common element. In the high-temperature deformation the edges stacked along c are all displaced in the same way, whereas neighboring edges are displaced in opposite senses below the SP transition resulting in the twist distortion. That both deformations reflect related structural instabilities is supported

by the fact that for both distortions the strongest influence is found for b which decreases with decreasing temperature in both cases.

Although several groups performed single-crystal Raman analyses²⁶⁻²⁸ above and below T_{SP} , it remains still unclear whether there exists a soft phonon mode close to T_{SP} . An intensity near 30 cm^{-1} appearing at T_{SP} was interpreted as being due to a soft phonon mode.²⁶ However, more detailed studies^{27,28} indicated a magnetic origin for this intensity. Also recent inelastic neutron-scattering studies were unable to reveal softening phonon modes in the neighborhood of the SP superstructure peaks.²⁹ The phonon mode associated with the high-temperature dependence of the Pbm structure should belong to the A_g representation. In the CuGeO_3 structure there should be four modes of this symmetry and all of them were determined by Raman scattering;²⁷ none of them possesses a low frequency. Hence, the displacement pattern shown in Fig. 4(a) without the concomitant reduction of the b axis appears rather rigid.

Rather anomalous features were observed by electron diffraction. Kamimura *et al.*¹⁰ and Chen and Cheong³⁰ report diffuse intensity which is sharp along the b direction, broadened along a and with almost no modulation at all along c , and which passes through the $(0 k 0)$ $k \neq 0$ Bragg peaks. Both groups conclude that this intensity cannot be interpreted as a precursor of the SP transition as no maxima near $l = (n/2)$ are found. The structural deformation observed as a function of temperature might be related to these diffuse streaks. The twist or rotation deformations of the $\text{Cu}[\text{O}(2)]_2$ ribbons are rather strongly coupled along b and almost free along c which agrees with the orientation of the diffuse streaks. A local O(2)-O(2) edge rotation distortion might further explain the rather large thermal ellipsoids of the O(2) site in the direction almost perpendicular to the edges. This mean-square displacement remains elevated even at low temperatures which cannot be explained within harmonic lattice dynamics. That the shift during the SP transition is not perpendicular to the O(2)-O(2) edge, but to the GeO(2) bond, supports the conclusion in Refs. 10 and 30 that the deformations above T_{SP} are not directly related to the SP transition itself.

C. Relation between bond angles and magnetic interaction

Figure 5 shows the orbitals which are expected to be essential for the magnetic interaction in the Cu chains along c . The main antiferromagnetic interaction is given by the superexchange paths Cu-O(2)-Cu, which present an angle η of 90° for the ideal configuration with quadratic $\text{Cu}[\text{O}(2)]_4$ units. In the ideal situation with $\eta = 90^\circ$, however, there is no effective exchange; the antiferromagnetic interaction should cancel out in this case leading to a weak ferromagnetic interaction.³¹ As described above, the $\text{Cu}[\text{O}(2)]_4$ squares are deformed into rectangles the ratio of the long to the short edge being 1.2. Therefore, the Cu-O(2)-Cu bond angle η deviates strongly from 90° , and the antiferromagnetic interaction is induced.

In the following we present a more quantitative evaluation of J as a function of the atomic arrangement; a detailed description of the model used will be given elsewhere.³²

In order to compute J we consider a cluster consisting of two adjacent Cu in a chain, and the two O ligands in between and the two Ge nearest to the latter (Fig. 5). We choose a

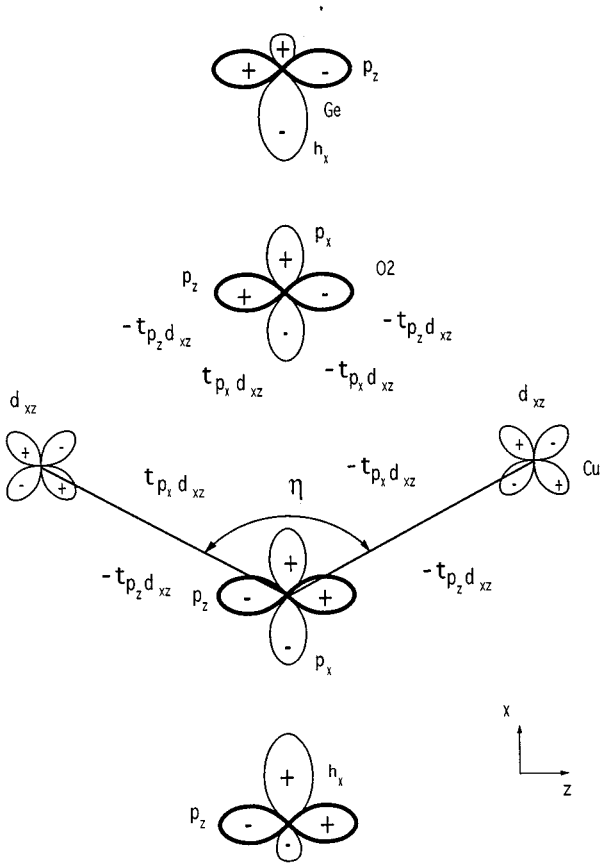


FIG. 5. Orbitals used in the computation of J . The z axis corresponds to the chain direction, the x direction is parallel to the $\text{Cu}[\text{O}(2)]_4$ planes. h_x denotes an s - p hybrid.

coordinate system with z parallel to the chains and x parallel to the $\text{Cu}[\text{O}(2)]_4$ octahedron basal plane.

The electronic part of the Hamiltonian we consider is

$$\begin{aligned}
 H = & \sum_{i \neq j, \sigma} t_{ij} c_{i\sigma}^\dagger c_{j\sigma} + \sum_{i, \sigma} U_i c_{i\sigma}^\dagger c_{i\sigma} + \sum_i U_i c_{i\downarrow}^\dagger c_{i\downarrow} c_{i\uparrow}^\dagger c_{i\uparrow} \\
 & + \sum_{\langle i \neq j \rangle, \sigma, \sigma'} U_{ij} c_{j\sigma'}^\dagger c_{j\sigma'} c_{i\sigma}^\dagger c_{i\sigma} \\
 & + \sum_{\langle i \neq j \rangle, \sigma, \sigma'} K_{ij} c_{i\sigma}^\dagger c_{i\sigma'} c_{j\sigma'}^\dagger c_{j\sigma}, \quad (1)
 \end{aligned}$$

where the operator $c_{i\sigma}^\dagger$ creates a *hole* of spin σ and the index i runs through the Cu d_{xz} , the O $p_{x,z}$ and the Ge s, p orbitals.

e_i and t_{ij} are single-particle and hopping matrix elements, respectively. Holes repel each other with strength U_i on orbital i and strength U_{ij} between different orbitals i and j . K_{ij} is the exchange interaction between different orbitals (usually ferromagnetic). On-site and intersite nonzero matrix elements are shown in Table IV.

The hopping matrix element between the O(2) p_x or p_z orbital and the Cu d_{xz} is given in terms of Slater and Koster integrals^{37(a)} (SKI) by

$$t_{p_x d_{xz}} = \sqrt{3} l m^2 (p d \sigma) - l (1 - 2 m^2) (p d \pi), \quad (2)$$

$$t_{p_z d_{xz}} = \sqrt{3} m l^2 (p d \sigma) - m (1 - 2 l^2) (p d \pi),$$

where $m = \cos(\eta/2)$, $l = \sin(\eta/2)$. This dependence will prove to be very important to determine the dependence of J on structural changes. We also take Harrison^{37(b)} like dependences of the hopping matrix elements on lattice displacements and point-charge estimate dependences of the on-site energies on lattice displacements. The effect of the last two resulted to be negligible in determining the structural dependence of J . If one neglects hybridization, the Cu is in the d^9 configuration with one hole in the d_{xz} orbital and the O's have closed shells.

The computation technique is similar to the case of the parent superconducting cuprates (SC).³⁸ In order to simplify the problem we construct s - p hybrid orbitals in Ge and do a canonical transformation to eliminate the single-particle states that do not mix with the d_{xy} orbital because of symmetry (i.e., the linear combination of the O and Ge orbitals that have opposite parity respect to the d_{xz} orbital) or are too far in energy [antibonding combinations of Ge and O(2) orbitals]. This is on the same line as the cell perturbation approach used in the cuprates.^{37(b)} The resulting Hamiltonian is diagonalized *exactly* and J is computed as the energy difference between the lowest-energy singlet state and the lowest-energy triplet state. We found that although a perturbative expression in t_{ij} is useful to analyze the qualitative behavior and identify the different processes, it gives very bad quantitative results, typically a factor of 2 or more larger than the exact value obtained by diagonalizing the matrixes. This is due to the strong covalency and because the effect of the two different p orbitals tend to cancel each other so that an error in each contribution gets amplified.

If we neglect the Ge orbitals, set $K_{ij}=0$ and put $U_p = U_{p_z p_x}$ we get that for $\eta=90^\circ$, $J(90^\circ)=0$. This can be easily understood by rotating the p orbitals by 45° . In this situation each Cu orbital mixes with a different set of O orbitals, which are mutually orthogonal, and superexchange is not possible.³¹ If the Hund's rule exchange in the ligand $J_{p_x p_z} > 0$ or $U_p > U_{zx}$, a ferromagnetic interaction results. However, the tendency to ferromagnetism from these terms is not very strong since in a perturbative expansion they act in fourth order in t_{ij} . By contrast $K < 0$ produces a strong tendency to ferromagnetism since it acts on second order.

The effect of the Ge is to make the ligand orbitals in the x and z direction nonequivalent. This makes the curve of J vs η asymmetric with respect to 90° because of the nonequivalence of the respective exchange paths.

Now we fix the angle at the ideal low-temperature undistorted value defined as $\eta^0 = (\eta^a + \eta^b)/2$, see Table III. This value of η is indicated by the vertical line in Fig. 6.

Setting $K_{pd}=0$ and the other parameters as in Table IV one gets a strong antiferromagnetic J . In fact in this situation $t_{p_x d_{xz}} = 0.6$ eV, $t_{p_z d_{xz}} = 0.8$ eV quite far from the ideal 90° situation ($t_{p_x d_{xz}} = t_{p_z d_{xz}}$), [see Fig. 6(b)]. J for these parameters is typically ~ 50 meV, i.e., \sim five times larger than the experimental one.⁶ One might ascribe that discrepancy to the uncertainty in the parameters, however, within reasonable

TABLE IV. Parameters used in the calculations. All the parameters are appropriate for holes. SKI were taken from local-density-approximation (LDA) (Ref. 33) estimates. Our experience from the parent superconducting cuprates is that LDA tend to overestimate hybridizations by $\sim 15\%$ respect empirical estimates (Ref. 34). Accordingly we apply that reduction to the LDA estimates. Coulomb parameters are taken similar to those in the PSC (Refs. 34 and 35) when known or reasonable estimates when not known. For closed-shell orbitals we take the LDA on-site energies. The Cu level was fixed by requiring that the energy difference between Cu d_{xz} and the ligands orbitals give a charge-transfer gap somewhat smaller than in the cuprates as seen in optical absorption (Ref. 36).

On-site	Cu	O(2)	Ge
e_i	$e_d = -0.5$	$e_p = 2.6$	$e_s = 1.0, e_p = -5.0$
U_i	$U_d = 8.0$	$U_p = 4.0$	
U_{ij}		$U_{p_x p_z} = 3.2$	
$-K_{ij}$		$J_{p_x p_z} = 0.6$	
Intersite	Cu-O(2)	O(2)-O(2)	Ge-O(2)
t_{ij}	$\pm t_{p_x d_{xz}}, \pm t_{p_z d_{xz}}$ ^a ($pp\sigma$) = -1.2, ($pp\pi$) = -0.3 ^b ($pp\sigma$) n = -3.0, ($sp\sigma$) n = -2.35 ^c ($pp\pi$) = 1.2,		
U_{ij}	$U_{pd} = 0.56$		
$-K_{ij}$	$-K_{pd} = 0.11$		

^aSee Eq. (2), here ($pd\sigma$) = 1.2, ($pd\pi$) = -0.5 and the sign are shown in Fig. 5.

^bThis was not given in Ref. 33 so was estimated by adjusting the values (Refs. 34 and 35) in the PSC with Harrison relations (Ref. 37b).

^c $n = \cos\theta$, where $\theta = 20^\circ$ is the angle between the Ge-O(2) and the CuO(2) basal plane.

variations and keeping $K_{pd} = 0$, the discrepancy remains. This means that the anomalously small J value is not due to the closeness to the ideal 90° situation alone. By putting $K_{pd} = -0.11$ eV, one gets an almost perfect cancellation of the antiferromagnetic contribution with $J = 13.2$ meV close to the experimental value. The effect of K is to produce an almost rigid vertical translation of the curve in Fig. 6 so that for $K = -0.11$ eV the point where the curve crosses the hori-

zontal axis is very close to η^0 . In this situation a 10% variation in K produces a 100% variation in J . This extreme sensitivity to K , perhaps the least known parameter in the problem, makes an *ab initio* computation of J a fruitless task. Instead we have taken a reasonable set of parameters leaving K free and then varied K to get a value of J close to the experimental one. The resulting value $K = -0.11$ eV is quite reasonable given that in the SC a value of $K = -0.22$ eV was estimated when the O orbitals point towards the Cu.³⁹ This parameter is also important in the SC (Refs. 38 and 39) but not so dramatic as for CuGeO_3 . We remark that in contrast to this strong sensitivity of J on K_{pd} we find that the derivative of J with respect to lattice distortions depends very weakly on the chosen parameter sets (less than 30% variations for physically mining full change in the parameters). This allows us to study the influence of the structure on J .

We want first to analyze the influence of the temperature dependency of η in the $Pbmm$ phase above T_{SP} . In fact the small variation of η results in a rather strong shift: for the value of η at 20 K we find $J = 13.7$ meV, and for the value of η at 295 K, $J = 12.5$ meV. Although this is significant enough to have consequences in the temperature-dependent properties like the susceptibility we do not think that it can explain the anomalous observations in those properties.² In particular at low temperature the decrease of J with T should lead to an enhanced slope of the susceptibility which is in contradiction to the experiment. Instead a model with a second-nearest-neighbor coupling seems to explain these results.⁴⁰ Riera and Dobry⁴⁰ needed a J_{NNN}/J ratio close to 0.36, which appears rather reasonable. The next-neighbor superexchange path for this process goes through Cu-O(2)-O(2)-Cu as suggested in Ref. 7. The geometry is almost identical to the one for J_{NNN} in the SC. So one expects a J_{NNN} of similar magnitude. There J_{NNN} is estimated to be ~ 10 meV,⁴¹ i.e., of the same order of magnitude as J in CuGeO_3 .

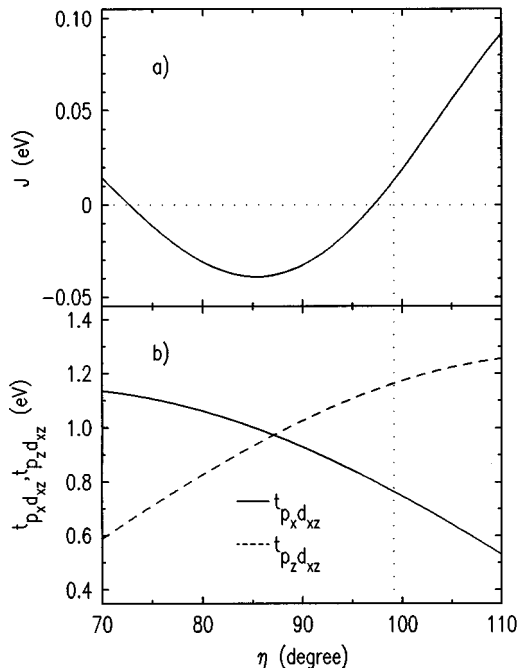


FIG. 6. (a) J as a function of η in the exact calculation (full line). (b) $t_{p_z d_{xz}}$ (dashed line) and $t_{p_x d_{xz}}$ (full line) hopping matrix elements as a function of η .

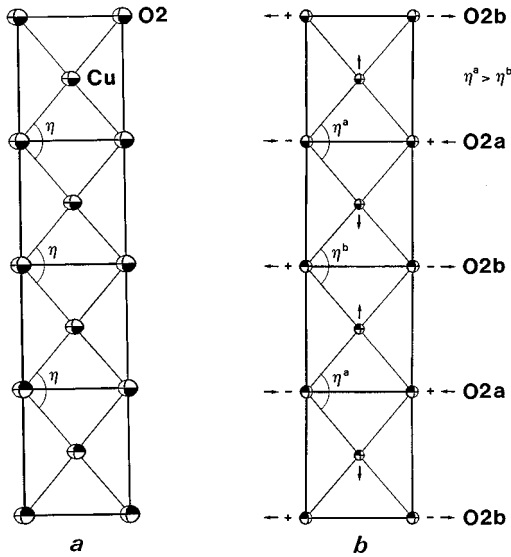


FIG. 7. Arrangement of the Cu and O(2) sites in the Cu chains in the form of an ORTEP plot with viewing direction perpendicular to the $\text{Cu}[\text{O}(2)]_4$ squares. (a) presents the arrangement at room temperature, (b) that in the spin-Peierls phase (both with exact scale). The distortion of the O(2)-O(2) distances can be seen only by careful inspection. The arrows and the + and - signs illustrate qualitatively the atomic shifts perpendicular and parallel to the drawing plane.

It remains unclear which interaction would be the driving element for the structural temperature dependence. The structural instability might induce changes in J or a change in J might be favorable in order to reduce the magnetic free energy and hence induce the structural deformation. The magnetic origin of this effect is supported by the fact that the extrema in the thermal expansion occur at rather low temperatures; whereas the similar behavior on applying pressure at room temperature indicates a purely structural instability.¹⁵ Structural high-temperature studies would be valuable in order to clarify the importance of the magneto-elastic coupling.

The $\text{CuO}(2)$ arrangement in the spin-Peierls phase is more complex: due to the opposite shifts the Cu and O(2) atoms are no longer in a plane as indicated by the + and - signs in Fig. 7(b). Additionally, the O(2a)-O(2a) edges are shorter than the O(2b)-O(2b) edges and the Cu site is displaced towards O(2b)-O(2b). The distortion shifts the O(2)-Cu-O(2) bond angles drastically: for O(2a), the angle η^a increases to 99.59° , whereas it decreases for O(2b), $\eta^b = 98.76^\circ$. For these values we get $J^a = 16.0$ meV and $J^b = 10.4$ meV which gives the dimerization parameter, $|J^{a,b} - J^0| = 2.8$ meV. This value is comparable to the mean-field estimate⁴ but much larger than theoretical estimates ($|J^{a,b} - J^0| \sim 0.4$ meV) based on the fitting of inelastic neutron-scattering experiments under the assumption that the chains can be treated independently.⁴² We have tried different parameter sets but the dimerization values obtained are always much larger than those estimates. We believe that this discrepancy is due to the neglectance of the interchain coupling (J_\perp) in Ref. 42. The importance of interchange coupling was emphasized in Refs. 4 and 17. In fact it can be shown that J_\perp lowers the gap due to band motion of the triplet excitation.³² In addition

substantial interchain coupling will favor antiferromagnetism and presumably a much stronger value of the dimerization is, hence, needed to overcome that tendency.

We have also computed the change in J due to the small changes in the O(2)-O(2) the Cu-O(2) and Ge-O(2) distances. In all cases we find that the changes in J are an order of magnitude smaller. In this context it may be understood why the distortion at T_{SP} is only indirectly related to the structural instability which seems responsible for the temperature dependence and the diffuse scattering: the SP distortion scheme has a more pronounced effect on η and, hence, appears favorable in order to produce a large dimerization parameter.

V. CONCLUSION

The structural analysis of CuGeO_3 as a function of temperature reveals rather anomalous effects already above T_{SP} . In accordance with the unusual thermal expansion, CuGeO_3 exhibits important structural modifications on cooling down to 20 K. The deformation can be characterized by a rotation of the $\text{Cu}[\text{O}(2)]_2$ ribbons around the c axis with accompanying translational shifts of the GeO_4 tetrahedra. Additionally, a temperature-dependent distortion of the octahedron basal plane, $\text{Cu}[\text{O}(2)]_4$, is observed, which may explain the anomalous behavior of the thermal expansion along a and c . As the superexchange interaction between neighboring Cu's is very sensitive to the surrounding bond angles, the distortions in the P4mm phase have a strong impact on the magnetic interaction parameter J . In this context it might be necessary to take them into consideration for a quantitative description of the magnetic susceptibility above T_{SP} , even though the observed effect appears unable to explain the discrepancy between the observed susceptibility and Bonner-Fischer theory.²

The structure in the spin-Peierls phase confirms the model proposed by Hirota *et al.*,¹¹ with a different direction for the O(2) site shifts. The distortion scheme in the SP phase differs from the deformations above T_{SP} ; it may roughly be characterized by a rotation of the GeO_4 tetrahedra. However, both deformations consist of rotational distortions of the octahedron O(2)-O(2) edges around the c axis. The temperature-dependent and the spin-Peierls deformation might reflect the same structural instability characterized by twisting of the O(2)-O(2) octahedron edges. The analysis of the anisotropic mean-square displacements indicates that only the temperature-dependent deformation above T_{SP} may be related to the diffuse scattering observed in electron diffraction.¹⁰ In contrast, the structural distortion at T_{SP} optimizes the splitting in the magnetic interaction parameter J due to the important modulation of the O(2)-Cu-O(2) angle in the superexchange path.

ACKNOWLEDGMENTS

We thank B. Büchner, B. Hennion, and W. Reichardt for valuable discussions. A.R. and G.D. acknowledge support by NEDO.

- ¹See, for example, *Organic and Inorganic Low Dimensional Crystalline Material*, Vol. 168 of *NATO ASI Series B*, edited by P. Delhaes and M. Drillon (Plenum, New York, 1987).
- ²M. Hase, I. Terasaki, and K. Uchinokura, *Phys. Rev. Lett.* **70**, 3651 (1993).
- ³M. Hase, I. Terasaki, K. Uchinokura, M. Tokunaga, N. Miura, and H. Obara, *Phys. Rev. B* **48**, 9616 (1993).
- ⁴M. Nishi, O. Fujita, and J. Akimitsu, *Phys. Rev. B* **50**, 6508 (1994).
- ⁵J. C. Bonner and M. E. Fisher, *Phys. Rev.* **135**, A640 (1964).
- ⁶M. Nishi, *J. Phys. Condens. Matter* **6**, L19 (1994).
- ⁷J. E. Lorenzo, K. Hirota, G. Shirane, J. M. Tranquada, M. Hase, K. Uchinokura, H. Kojima, I. Tanaka, and Y. Shibuya, *Phys. Rev. B* **50**, 1278 (1994).
- ⁸J. P. Pouget, L. P. Regnault, M. Ain, B. Hennion, J. P. Renard, P. Veillet, G. Dhalenne, and A. Revcolevschi, *Phys. Rev. Lett.* **72**, 4037 (1994).
- ⁹J. P. Renard, K. Le Dang, P. Veillet, G. Dhalenne, A. Revcolevschi, and L. P. Regnault, *Europhys. Lett.* **30**, 475 (1995).
- ¹⁰O. Kamimura, M. Terauchi, M. Tanaka, O. Fujita, and J. Akimitsu, *J. Phys. Soc. Jpn.* **63**, 2467 (1994).
- ¹¹K. Hirota, D. E. Cox, J. E. Lorenzo, G. Shirane, J. M. Tranquada, M. Hase, K. Uchinokura, H. Kojima, Y. Shibuya, and I. Tanaka, *Phys. Rev. Lett.* **73**, 736 (1994).
- ¹²H. Völlenkle, A. Wittmann, and H. Nowotny, *Monatsh. Chem.* **98**, 1352 (1967).
- ¹³H. Winkelmann, E. Gamper, B. Büchner, M. Braden, A. Revcolevschi, and G. Dhalenne, *Phys. Rev. B* **51**, 12 884 (1994).
- ¹⁴M. Poirier, M. Castonguay, A. Revcolevschi, and G. Dhalenne, *Phys. Rev. B* **51**, 6147 (1995).
- ¹⁵D. M. Adams, J. Haines, and S. Leonard, *J. Phys. Condens. Matter* **3**, 5183 (1991).
- ¹⁶A. Revcolevschi and G. Dhalenne, *Adv. Mater.* **5**, 9657 (1994).
- ¹⁷T. M. Brill, J. P. Boucher, J. Voiron, G. Dhalenne, A. Revcolevschi, and J. P. Renard, *Phys. Rev. Lett.* **73**, 1545 (1994).
- ¹⁸E. I. Speranskaya, *Izv. Akad. Nauk SSSR, Neorg. Mater.* **3**, 1458 (1967).
- ¹⁹U. H. Zucker, E. Perrenthaler, W. F. Kuhs, R. Bachmann, and H. Schulz, *J. Appl. Crystallogr.* **16**, 358 (1983).
- ²⁰M. A. Green, M. Kurmoo, J. K. Stalick, and P. Day, *J. Chem. Soc. Chem. Commun.* **17**, 1995 (1994).
- ²¹B. Roessli, P. Fischer, J. Schefer, W. Bühner, A. Furrer, T. Vogt, G. Petravovski, and K. Sablina, *J. Phys. Condens. Matter* **6**, 8469 (1994).
- ²²M. Arai, M. Fujita, K. Ubukata, T. Bokui, K. Tabata, H. Ohta, M. Motokawa, T. Otomo, K. Ohyama, M. Mino, J. Akimitsu, and O. Fujita, *J. Phys. Soc. Jpn.* **63**, 1661 (1994).
- ²³M. Braden, G. Heger, P. Schweiss, Z. Fisk, K. Gamayunov, I. Tanaka, and H. Kojima, *Physica C* **191**, 455 (1992).
- ²⁴I. D. Brown and D. Altermatt, *Acta Crystallogr. A* **32**, 751 (1976).
- ²⁵For example, R. J. Cava, A. Santoro, D. W. Johnson, and W. W. Rhodes, *Phys. Rev. B* **35**, 6716 (1987); M. Braden, P. Schweiss, G. Heger, W. Reichardt, Z. Fisk, K. Gamayunov, I. Tanaka, and H. Kojima, *Physica C* **223**, 396 (1994).
- ²⁶S. Sugai, *J. Phys. Soc. Jpn.* **62**, 3829 (1994).
- ²⁷M. Udagawa, H. Aoki, N. Ogita, O. Fujita, A. Sohma, A. Ogihara, and J. Akimitsu, *J. Phys. Soc. Jpn.* **63**, 4060 (1994).
- ²⁸H. Kuroe, T. Sekine, M. Hase, Y. Sasago, K. Uchinokura, H. Kojima, I. Tanaka, and Y. Shibuya, *Phys. Rev. B* **50**, 16 468 (1994).
- ²⁹B. Hennion and M. Ain (unpublished).
- ³⁰C. H. Chen and S.-W. Cheong, *Phys. Rev. B* **51**, 6777 (1995).
- ³¹J. B. Goodenough, *Magnetism and Chemical Bond* (Interscience, New York, 1963).
- ³²J. Lorenzana (unpublished).
- ³³L. F. Mattheiss, *Phys. Rev. B* **49**, 14 050 (1994).
- ³⁴H. Eskes, G. Sawatzky, and L. Feiner, *Physica C* **160**, 424 (1989); and references therein.
- ³⁵A. K. McMahan, J. F. Annett, and R. M. Martin, *Phys. Rev. B* **42**, 6268 (1990).
- ³⁶I. Terasaki, R. Itti, N. Koshizuka, M. Hase, I. Tsukuda, and K. Uchinokura, *Phys. Rev. B* **52**, 295 (1995).
- ³⁷(a) J. C. Slater and G. F. Koster, *Phys. Rev. B* **94**, 1498 (1954) (b) W. A. Harrison, *Electronic Structure and the Properties of Solids* (Freeman, San Francisco, 1980).
- ³⁸(a) H. Eskes and J. H. Jefferson, *Phys. Rev. B* **48**, 9788 (1993); (b) J. H. Jefferson, H. Eskes and L. F. Feiner, *ibid.* **45**, 7959 (1992).
- ³⁹E. B. Stechel and D. R. Jennison, *Phys. Rev. B* **38**, 4632 (1988).
- ⁴⁰J. Riera and A. Dobry, *Phys. Rev. B* **51**, 16 098 (1995).
- ⁴¹J. F. Annett, R. M. Martin, A. K. McMahan, and S. Satpathy, *Phys. Rev. B* **40**, 2620 (1989).
- ⁴²G. Castilla, S. Chakravarty, and V. Emery, *Phys. Rev. Lett.* **75**, 1823 (1995).